J Mater Sci: Mater Med (2011) 22:2727–2734
DOI 10.1007/s10856-011-4465-6

Influence of microstructure and chemical composition of sputter deposited TiO_2 thin films on in vitro bioactivity

Mirjam Lilja · Axel Genvad · Maria Åstrand · Maria Strømme · Håkan Enqvist

Received: 2 June 2011 / Accepted: 17 October 2011 / Published online: 4 November 2011

Abstract Functionalisation of biomedical implants via surface modifications for tailored tissue response is a growing field of research. Crystalline TiO_2 has been proven to be a bone bioactive, non-resorbable material. In contact with body fluids a hydroxyapaptite (HA) layer forms on its surface facilitating the bone contact. Thus, the path of improving biomedical implants via deposition of crystalline TiO_2 on the surface is interesting to follow. In this study we have evaluated the influence of microstructure and chemical composition of sputter deposited titanium oxide thin films on the in vitro bioactivity. We find that both substrate bias, topography and the flow ratio of the gases used during sputtering affect the HA layer formed on the films after immersion in simulated body fluid at 37°C. A random distribution of anatase and rutile crystals, formed at negative substrate bias and low Ar to O_2 gas flow ratios, are shown to favor the growth of flat HA crystal structures whereas higher flow ratios and positive substrate bias induced growth of more spherical HA structures. These findings should provide valuable information when optimizing the bioactivity of titanium oxide coatings as well as for tailoring process parameters for sputtered-based production of bioactive titanium oxide implant surfaces.

M. Lilja · M. Strømme (✉)
Division for Nanotechnology and Functional Materials, Department of Engineering Sciences, The Ångström Laboratory, Uppsala University, Box 534, 75121 Uppsala, Sweden
e-mail: maria.stromme@angstrom.uu.se

M. Lilja · M. Åstrand
Sandvik Tooling Sverige AB, Lerkrogsvägen 19, 12680 Stockholm, Sweden

A. Genvad · H. Enqvist (✉)
Division of Applied Materials Science, Department of Engineering Sciences, The Ångström Laboratory, Uppsala University, Box 534, 75121 Uppsala, Sweden
e-mail: hakan.engqvist@angstrom.uu.se

1 Introduction

Titanium is widely used in medical applications due to its excellent biocompatibility, good mechanical strength and due to its inertness in biological systems [1]. When exposed to air, titanium is—in contrast—highly reactive and is immediately covered by a few nanometer thick amorphous oxide layer, which has proven to be essential for the inert body response [2]. To further improve the bone response to titanium, the surface can be coated with a bioactive material such as bioglass [3], hydroxyapatite (HA) [4] and ceramic apatite-wollastonite [5]. Bioactive materials spontaneously bond to living bone and are clinically used as bone substitutes [6–9].

Crystalline TiO_2 is also known as a bioactive, non-resorbable, material. A bioactive HA layer spontaneously forms on its surface upon contact with body fluids [1, 10].

Except from the rare high-pressure forms, crystalline TiO_2 occurs in nature in two tetragonal phases, rutile and anatase, as well as in the orthorhombic phase, brookite. The most common form is rutile, which is thermodynamically stable at all temperatures and has the highest density of the three phases [11]. Anatase is kinetically stable in the nanocrystalline form at lower temperatures but transforms into rutile at temperatures above 900°C [12]. Both anatase and rutile have well-documented ability to form bioactive HA layers in vitro [13–18], and also brookite has been indicated to possess similar properties [19].

A critical characteristic of a bioactive material is the ability to form bone-like apatite on the surface when implanted in the body [20, 21]. It has been proven that materials, which form

HA on the surface when submerged in simulated body fluids, such as Phosphate Buffer Saline (PBS), also form HA in the body [21]. Hence, in vivo bone bioactivity can be predicted with a simple in vitro PBS-test [21].

Functionalisation of implant surfaces via HA-coatings offers one way to provide bioactive surfaces promoting integration of the implant. While commercially available plasma spraying results in HA coatings having low crystallinity, large porosity and poor adherence to the substrate [22], conventional sputtering techniques have shown some advantages with respect to adherence and density [23]. As-sputtered films are usually amorphous and can cause excessive dissolution in a physiological environment and thereby reduce the film integrity of the implants [24, 25]. To decrease the solubility of amorphous HA coatings, the crystallinity needs to be enhanced by post-deposition annealing [26, 27].

Thus, deposition of thin, crystalline TiO_2 coatings on mechanically strong substrates is considered an attractive way to provide materials with good mechanical and bone bonding properties for long-term clinical use [22, 28]. Physical Vapor Deposition (PVD) techniques, such as diode (DC) and radio frequency (RF) magnetron sputtering allow for tailoring of the structure design while providing large area uniformity and strong substrate adhesion [29, 30]. In comparison to sol–gel methods, no post-temperature treatment is required for surface functionalisation. The high deposition rate of DC magnetron sputtering, employing argon as the inert sputtering gas, makes this coating technique especially attractive for large-scale industrial production. The structural and compositional properties of magnetron sputtered films depend on several deposition conditions with the Ar to O_2 gas flow ratio being one of the important parameters [31, 32]. Over the past few years, the deposition of reactive pulse magnetron sputtering has been investigated. These studies focused on tailoring the film growth by selecting the appropriate process conditions and pulse parameters [33–35]. The influence of bias voltage on the bioactivity has been studied for low temperature TiO_2 sputtered films by Kasemanankul et al. [36]. A higher density and degree of crystallinity of formed HA was observed on TiO_2 films deposited at low bias voltage. To our knowledge, however, no attempts has been made to establish a correlation between bioactivity and the physical properties of magnetron sputtered TiO_2 thin films deposited using different Ar to O_2 gas flow ratios.

The aim of the work presented in this paper is, thus, to synthesize crystalline TiO_2 coatings at different Ar to O_2 gas ratios by means of DC magnetron sputtering and to evaluate them with respect to their in vitro bioactivity. Crystal structure, microstructure, morphology and chemical composition are evaluated using X-ray Diffraction (XRD), Scanning Electron Microscopy (SEM), Energy Dispersive X-ray Spectroscopy (EDS) and X-ray Photoemission Spectroscopy (XPS). The bioactivity is evaluated using SEM and XRD after 7 days in PBS.

2 Experimental

2.1 Substrates

Square samples (1 × 20 × 20 mm) of commercially pure titanium (grade 2), Ti_6Al_4V (grade 5) and stainless steel of medical grade AISI type 316L were used for coating depositions. Silicon-(110) wafers served as substrates for coating thickness measurements.

2.2 Thin film deposition

Before coating deposition, the substrates were ultrasonically cleaned for 6 min in an alkaline cleaning agent (UPON, pH 11.6) and thereafter rinsed meticulously under running deionized water and subsequently cleaned ultrasonically in ethanol for 6 min. In a final step, the samples were rinsed in ethanol and dried in pure nitrogen gas.

The coating series were deposited using a Balzers BAI640R magnetron sputtering system. The samples were pre-heated for 60 min at 200°C at a pressure of 2.5×10^{-3} mbar and Ar-etched for 6 min at 1.5×10^{-3} mbar prior to deposition. A solid Ti target was used in the Ar/O_2 environment and a magnetron power of 2.5 kW was employed. The magnetron power was chosen to be relatively high, based on the conclusions in earlier reports [10]. The deposition time for all coatings was 40 min. In the coating series denoted 9010, 6040 and 3070 the ratio of Ar to O_2 gas flow was 90:10, 60:40 and 30:70, respectively, at a constant total gas pressure: $p_{tot} = 4.2\ 10^{-3}$ mbar. One set of coatings with negative substrate bias (−180 V), denoted "neg", and one set with a positive bias (+150 V), denoted "pos", were deposited for the 9010, and the 3070 samples. The experiments using a negative bias were performed at two different temperatures; ~320°C, denoted "H" as in High temperature, and ~230°C, denoted "L" as in Low temperature. A batch deposited at an Ar to O_2 ratio of 30:70 with negative bias and at ~320°C was, thus, denoted 3070negH. The 6040 batch was deposited using self bias (−20 V) only. Three identical runs were made to confirm the reproducibility of this particular experimental set up. The complete experimental matrix and nomenclature is presented in Table 1.

2.3 Structural and compositional characterization

Grazing angle XRD using a Siemens D5000 diffractometer, operated with 1° incidence angle, was used to analyze

Table 1 Sample deposition parameters

Coating parameters			Actual values			
$Ar:O_2$	Temp.	Bias	Series name(s)	U_{bias} (V)	T_{start} (°C)	T_{40}min (°C)
90:10	Low	Pos	9010pos	+150	200	175
		Neg	9010negL	−180	240	210
	High	Neg	9010negH	−180	290	325
60:40	Medium	Self bias	6040_01	−20	240	265
			6040_02	−20	240	265
			6040_03	−20	240	265
30:70	Low	Pos	3070pos	+150	200	160
		Neg	3070negL	−180	250	210
	High	Neg	3070negH	−180	260	350

the crystalline structure of the TiO_2 coatings. A step size of 0.1° and a scan step time of 5 s were chosen and the 2θ scan was recorded in selected intervals between 20 and 80° depending on the investigated crystal structure.

The thicknesses of all TiO_2 coatings were measured by SEM on cross sections using a FEI Strata DB235 FIB/SEM. EDS analyses of the coatings were conducted in the SEM. Atomic concentrations of Ti and O at the surface were analyzed on a selection of samples by XPS in a Physical Electronics Quantum 2000 instrument with monochromatic Al Kα radiation (1486.7 eV) as the irradiating X-rays. The energy of the incident ions was 4 keV and the area of analysis was 2 mm × 2 mm. Pass energy was set to 187.85 eV and a step size of 0.8 eV was used. In total, four profiles were measured at increasing depths. Atomic concentrations were measured from each profile. As reference, a single crystalline rutile (001) sample was used.

2.4 In vitro bioactivity testing

All samples were taken directly out of the sputtering chamber and placed in small plastic zip-bags. From the zip bags they were put into centrifuge tubes filled with 42 ml PBS (Dulbecco's phosphate buffered saline), which is the maximum capacity of the tubes. The PBS has a pH of 7.4 at a temperature of 37°C. The tubes were kept in a controlled temperature of 37°C for 7 days and the samples were subsequently removed from the PBS, carefully rinsed in deionised water and left to dry in air before structural analysis. The in vitro bioactivity tests were repeated three times for each coating series. A Zeiss FEG-SEM LEO 1550 Gemeni was used for analysis of the HA surface structure as well as of the untreated substrates used for the titanium oxide deposition. The FEI Strata DB235 FIB/SEM was employed to make cross sections of two selected HA-coated samples.

3 Results and discussion

3.1 Crystallinity

Figure 1 shows XRD spectra of all three types of 9010-coatings under study. Wide peaks, corresponding to TiO, were clearly visible for the coatings deposited with negative bias; 9010negH and 9010negL. A slight shift in TiO-peak positions with respect to the reference peak positions was observed for both samples. It can also be observed that depositions with positive bias at low temperatures (sample 9010pos) lead to the formation of Ti_3O. The presence of Ti_3O for low temperature deposited coatings indicates an ordered, closed packed hexagonal (cph) phase as described earlier [37]. Neither anatase (A) nor rutile (R) peaks could be observed for any of the 9010 coatings. The atomic concentration of Ti in the 9010negL coating was found to be 47% from the XPS-analysis and 51% from the EDS analysis, see Table 2, which further confirms the presence of the TiO phase. Both XPS and EDS analyses performed on the 9010pos coatings

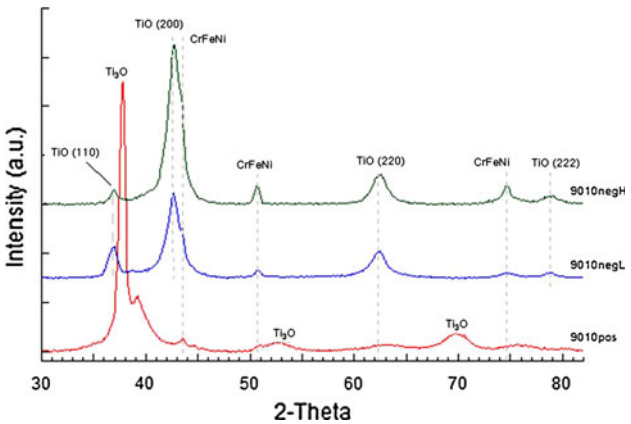

Fig. 1 XRD-diffractograms of the 9010 samples on stainless steel

Table 2 Results from coating analysis

Sample	TiO_2 thickness (nm)	At.% Ti XPS[a]	At.% Ti EDS	XRD pattern[b]	Biomimetic response
9010pos	2340	57	57	Ti_3O	No HA
9010negL	1650	47	51	TiO	No HA
9010negH	1590	–	–	TiO	No HA
6040_01	120	–	–	A(101)	Spherical
6040_02	140	29	–	A(101)	Spherical
6040_03	150	–	–	A(101)	Spherical
3070pos	170	–	–	A(101)	Flat
3070negL	180	32	–	R(101)	Flat
3070negH	140	31		R(101)	Spherical

[a] The presented values are average from the four depth profiles

[b] A and R denote the anatase and the rutile phase, respectively

revealed an atomic concentration of 43% oxygen, Table 2. The coating thickness of the 9010negL sample was about ~1.7 μm whereas the corresponding thickness of the 9010pos sample was ~2.3 μm and, thus, about 10 times thicker than the 6040 and 3070 samples, Table 2. This clearly indicated a metallic sputtering mode for the 9010 samples, i.e., the target sputter rate exceeded the oxidation rate of the target surface [38] and yielded relatively thick coatings of high Ti-content.

Figure 2 displays SEM recorded cross sections of a 9010pos and a 9010negL sample. As can be observed from the figure, the 9010pos coating has a columnar structure with a grain width significantly thinner than the coating thickness. The 9010negL coating is also columnar with increasing grain size towards the surface.

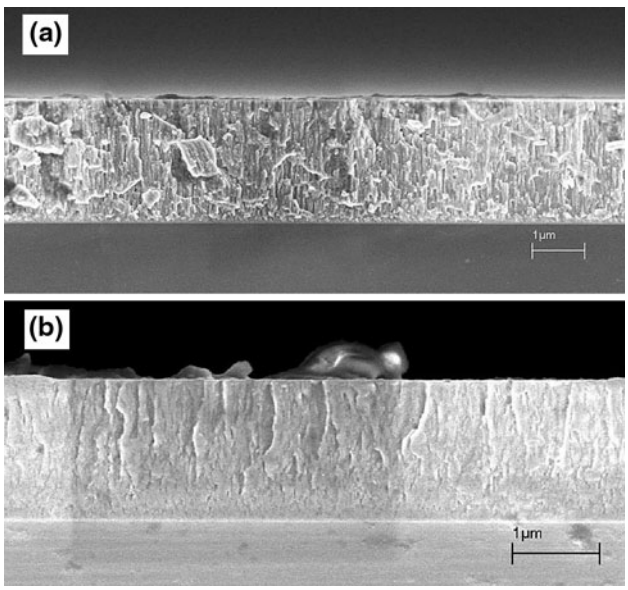

Fig. 2 SEM cross sections of **a** 9010pos and **b** 9010negL on Si

Diffractograms of the three identically deposited 6040 samples is presented in Fig. 3. Both anatase and rutile were detected with preferred orientation of the anatase (101). Low intensity TiO-peaks were also present. The atomic concentration of Ti in the coatings was found to be 29% as measured by XPS, see Table 2. Even if the samples were prepared under identical conditions, a slight variation in the diffractograms could be observed, e.g., rutile (101) could only be seen on the 6040_03 sample.

Figure 4 shows diffractograms for the 3070 samples. Wide rutile (101), (111) and (211) peaks could be detected in the 3070negL samples. On 3070negH only rutile (101) was detected. No formation of rutile (110), which has the

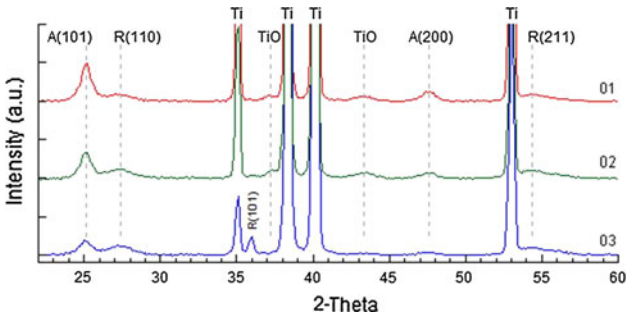

Fig. 3 XRD-diffractogram of the 6040 samples on grade 2 Ti

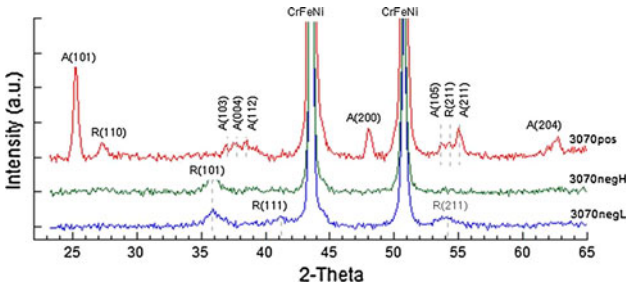

Fig. 4 XRD-diffractograms of the 3070 samples on stainless steel

lowest free energy [13], could be observed for the samples deposited using a negative bias. Positive bias under deposition leads to the formation of both anatase and rutile as evident from the diffractogram recorded on the 3070pos sample.

Figure 5 shows the SEM cross sections of a 3070negH and a 3070pos sample. Under negative bias a two layer structure, with a more fine grained structure close to the surface, can be observed. The 3070pos sample, on the other hand, shows a distinct columnar structure through the entire coating with a larger surface roughness as compared to the 3070negH coating. XPS recorded on the two types of 3070neg samples revealed an atomic concentration of Ti of 31–32%, cf. Table 2.

The above presented results clearly show on a large effect of the Ar to O_2 gas flow ratio on the microstructure evolution and chemical composition of magnetron sputtered titanium oxide coatings. A high Ar to O_2 gas flow ratio of 90:10 gave a metallic sputtering mode and, under negative bias, favored the formation of TiO. Positive bias further decreased the available amount of oxygen, which resulted in an even more metallic film with an oxygen concentration of 43% and a strong presence of Ti_3O.

At an Ar to O_2 gas flow ratio of 60:40, reactive sputtering occurred, leading to the formation of TiO_2. The low bias voltage (only self bias) used to deposit the 6040 coatings, allowed the formation of the lowest energy rutile and anatase phases; anatase (101) and rutile (110). Low intensity TiO peaks indicated a shortage of oxygen during deposition of these coatings.

At an increased oxygen flow, the influence of the bias voltage on the coating microstructure was prominent. On the 3070neg samples, rutile with preferred (101)-orientation was formed. The wide rutile (101) peak observed indicated that the grains were relatively small. Small grain size and strong orientation are signs of a large flux of impinging ions. The large negative bias seems to have contributed to suppressing the formation of anatase (101) and rutile (110), which is in good agreement with the results obtained by Song et al. [39] and Kasemandankul et al. [36]. In comparison to a highly negative charged substrate, high positive bias reduced the bombardment of Ar^+, which causes lower surface mobility [40] and allows for formation of the low energy rutile phase (110). The coating microstructure, formed at positive bias, showed a distinct columnar structure with less pronounced texture as compared to the coatings formed at negative bias, see Fig. 5. With respect to TiO_2-stoichiometry it can be concluded that the 3070pos deposition parameters are most optimal.

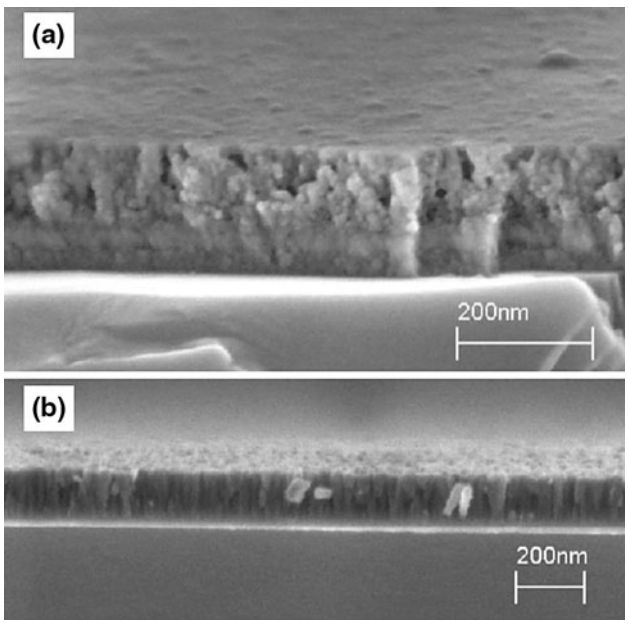

Fig. 5 SEM cross section of **a** 3070negH and **b** 3070pos on Si

3.2 Bioactivity

Table 2 presents a summary of the influence of microstructure and chemical composition on the HA formation and growth ability for all coating types investigated in this study. No HA was formed on any of the 9010-coatings after the in vitro bioactivity tests. Figure 6a, b show SEM images of the HA formed on a 3070negH and a 3070negL coating, respectively. As obvious from the panels, two different types of HA-growth were observed. On the 3070negL coating, HA grew in a flat "rug-like" structure while on 3070negH, as well as on the 6040 coatings (shown in Fig. 8 below), spherical formations of HA crystals could be observed. Both structures are covering the underlying titanium oxide completely.

Figure 6c, d display the FIB cross sections of a 3070negH and 3070negL sample after the bioactivity tests. While the average thickness of the flat HA structure on 3070negL is 4.6 ± 0.2 μm, an average thickness of 3.1 ± 0.2 μm was measured for the spherical HA structure on the 3070negH sample. XRD analysis confirmed that the structure seen on the samples after immersion in PBS was HA, see Fig. 7.

The influence of substrate morphology on the HA formation and growth can be observed in Fig. 8. A smoother surface topography, as seen for grade 5 Ti substrates (panel c) and stainless steel substrates (panel e) lead to a more uniform, even HA coating on the 6040 samples (panels d and f) compared to the rough underlying surface of grade 2 Ti (panel a) giving a more uneven HA structure (panel b).

While the microstructure and chemical composition appeared to be similar for the 3070negL and 3070negH coatings, they promoted different HA nucleation and

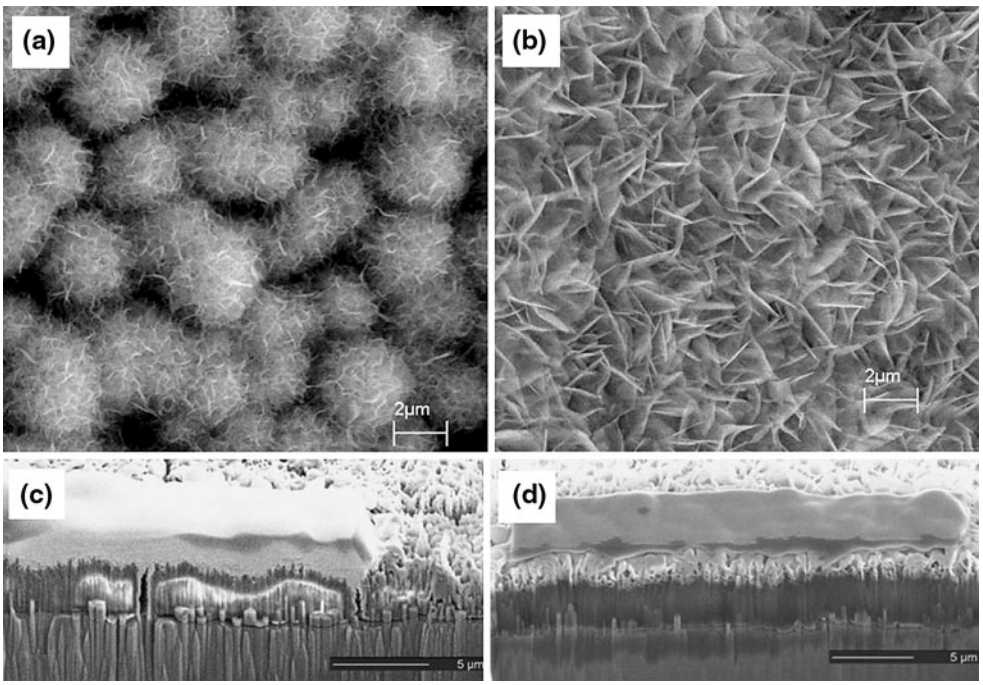

Fig. 6 SEM (**a**, **b** *scale bars* 2 μm) and FIB cross section (**c**, **d** *scale bars* 5 μm) images of spherical HA on 3070negH (**a**, **c**) and flat HA on 3070negL (**b**, **d**). Both coatings were deposited on grade 5 Ti

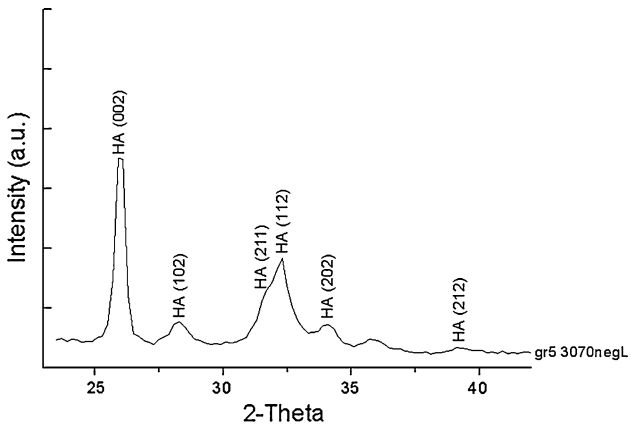

Fig. 7 XRD-diffractogram of HA formed on a 3070negL sample deposited on grade 5 Ti

growth, Fig. 7. This difference in HA morphology may be addressed to the titanium dioxide crystal orientation at the surface with the 3070negL samples having more variations in the rutile phase orientations as compared to the 3070negH samples. Different orientations could give different surface acidity and thereby change the number of available nucleation sites (i.e. deprotonated sites). Another explanation to the observed discrepancy could be differences in matching between the crystal orientation of the initially formed HA crystals and the crystal directions of the substrate surface resulting in a HA crystal starting to grow in a direction either vertical or horizontal to the surface. Spherical complexes are most likely to be formed when another HA-crystal nucleates on the first, as suggested by Lindahl et al. [41].

Flat HA growth, as seen on 3070pos samples, may be related to coating properties. Large crystal size and more randomly oriented crystals of both anatase and rutile may offer a more differentiated surface with higher crystallinity on which HA nucleates in flat structures.

4 Conclusions

The results obtained in this study show that DC magnetron sputtering offers a suitable deposition technique for synthesizing functional TiO_2 films. The best magnetron sputtered coatings, from a bioactivity aspect, were produced with positive target bias and an Ar to O_2 gas flow ratio of 30:70. Positive bias contributes to the growth of randomly oriented anatase and rutile crystals, with a large crystal size and a good bioactive response. Two different types of HA morphologies were identified on the TiO_2 surfaces after in vitro bioactivity testing; spherical and flat HA. It was concluded that substrate topography in combination with surface morphology and microstructure of the deposited TiO_2 thin films had an impact on HA nucleation and growth. Larger titanium oxide crystal size, smooth topography and more randomly oriented crystals of both anatase

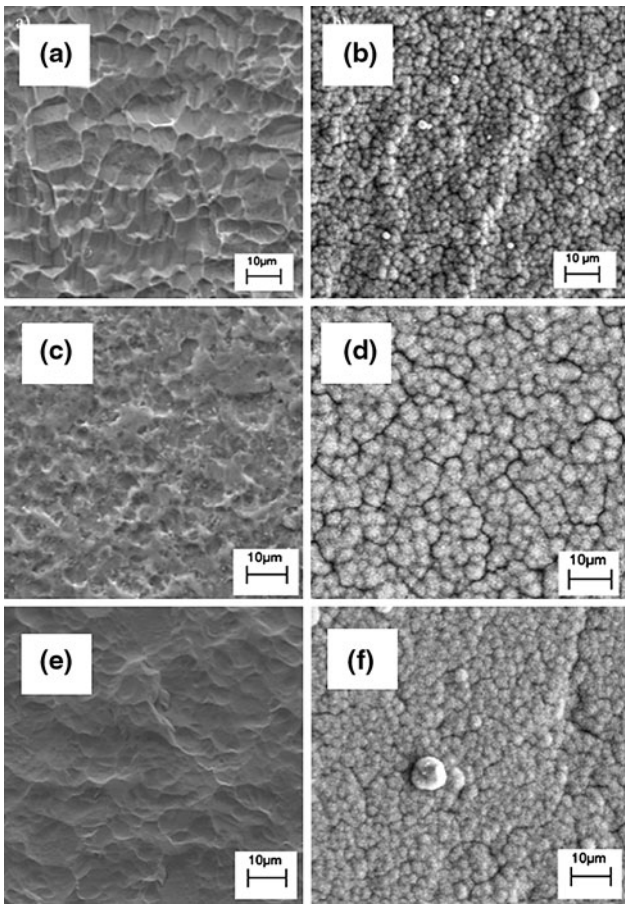

Fig. 8 SEM images of **a** untreated grade 2 Ti surface, **b** *spherical* HA on a grade 2 6040_01 sample, **c** untreated grade 5 Ti surface, **d** *spherical* HA on a grade 5 6040_01 sample, **e** untreated stainless steel and **f** *spherical* HA on a stainless steel 6040_01 sample

and rutile lead to the formation of flat HA crystals and a thicker HA film.

The findings presented in this paper should provide valuable information when optimizing the bioactivity of titanium oxide coatings as well as for tailoring process parameters for large scale production of bioactive titanium oxide implant surfaces using DC magnetron sputtering as deposition method.

References

1. Zhou W, Zhong X, Wu X, Yaun L, Shu Q, Xia Y, Ostrikov K. Plasma-controlled nanocrystallinity and phase composition of TiO_2: a smart way to enhance biomimetic response. J Biomed Mater Res. 2007;81A:453–64.
2. Ellingsen JE, Thomsen P, Lyngstadaas SP. Advances in dental implant materials and tissue regeneration. Periodontol 2000. 2006;41:136–56.
3. Hench LL, Splinter RJ, Allen WC, Greenlee TK. Bonding mechanisms at the interface of ceramic prosthetic materials. J Biomed Mater Res. 1971;5:117–41.
4. Jarcho M, Kay JL, Gumaer RH, Drobeck HP. Tissue, cellular and subcellular events at bone–ceramic hydroxyapatite interface. J Bioeng. 1977;1:79–92.
5. Kokubo T, Shigematsu S, Nagashima Y, Tashiro M, Nakamura T, Yamamuro T, et al. Apatite- and Wollastonite-containing glass–ceramics for prosthetic application. Bull Inst Chem Res. 1982; 60:260–8.
6. Kokubo T, Kim HM, Kawashita M. Novel bioactive materials with different mechanical properties. Biomaterials. 2003;24: 2161–75.
7. Kokubo T. Design of bioactive bone substitutes based on biomineralization process. Mater Sci Eng. 2005;C25:97–104.
8. Goto K, Tamura J, Shinzato S, Fujibayashi S. Bioactive bone cements containing nano-sized titania particles for use as bone substitutes. Biomaterials. 2005;33:6496–505.
9. Moore WR, Graves SE. Synthetic bone graft substitutes. ANZ J Surg. 2001;71:354–61.
10. Mihranyan A, Forsgren J, Strømme M, Engqvist H. Assessing surface area evolution during biomimetic growth of hydroxyapatite coatings. Langmuir. 2009;25:1292–5.
11. Zhou W, Zhong X, Wu X, Yaun L, Shu Q, Xia Y. Structural and optical properties of titanium oxide thin films deposited on unheated substrate at different total pressures by reactive magnetron Sputtering with a substrate bias. J Korean Phys Soc. 2006;49:2168–75.
12. Zhang Y, Ma X, Chen P, Yang D. Effect of the substrate temperature on the crystallization of TiO_2 films prepared by DC reactive magnetron sputtering. J Cryst Growth. 2007;300: 551–4.
13. Svetina M, Colombi Ciacchi L, Sbaizero O, Meriani S, De Vita A. Deposition of Calcium ions on rutile (110): a first principles investigation. Acta Mater. 2001;49:2169–77.
14. Keshmiri M. Apatite formation on TiO_2 anatase microspheres. J Non-Cryst Solids. 2003;324:289–94.
15. Piskounova S, Forsgren J, Brohede U, Engqvist H, Strømme M. In vitro characterization of bioactive titanium dioxide/hydroxyapatite surfaces functionalized with BMP-2. J Biomed Mater Res Part B Appl Biomater. 2009;91B:780–7.
16. Åberg J, Brohede U, Mihranyan A, Strømme M, Engqvist H. Bisphosphonate incorporation in surgical implant coatings by fast loading and co-precipitation at low drug concentrations. J Mater Sci Mater Med. 2009;20:2053–61.
17. Brohede U, Forsgren J, Roos S, Mihranyan A, Engqvist H, Strømme M. Multifunctional implant coatings providing possibilities for fast antibiotics loading with subsequent slow release. J Mater Sci Mater Med. 2009;20:1859–67.
18. Brohede U, Zhao S, Lindberg F, Mihranyan A, Forsgren J, Strømme M, Engqvist H. A novel graded bioactive coating on implant for enhanced fixation to bone. Appl Surf Sci. 2009;225: 7723–8.
19. Kokubo T, Matsushita T, Takadama H. Titania-based bioactive materials. J Eur Ceram Soc. 2007;27:1553–8.
20. Kokubo T, Kim HM , Kawashita M, Nakamura T. Bioactive metals: preparation and properties. J. Mater. Sci; Mater. Med. 2004;15:99–107.
21. Kokubo T, Takadama H. How useful is SBF in predicting in vivo bone bioactivity. Biomaterials. 2006;27:2907–15.
22. Liu X, Zhao X, Fu R, Ho JPY, Ding C, Chu PK. Plasma-treated nanostructured TiO_2 surface supporting biomimetic growth of apatite. Biomaterials. 2005;26:6143–50.
23. Thian ES, Huang J, Best SM, Barber ZH, Bonfield W. Magnetron co-sputtered silicon-containing hydroxyapatite thin films–an in vitro study. Biomaterials. 2005;26:2947–56.
24. Bauer TW, Geesink RCT, Zimmerman R, McMahon JT, Bone J. Hydroxyapatite-coated femoral stems: histological analysis of components retrieved at autopsy. J Surg. 1991;73A:1439–52.

25. Collier JP, Surprenant VA, Mayor MB, Wrona M, Jensen RE, Surprenant HP. Loss of hydroxyapatite coating on retrieved, total hip components. J Arthroplast. 1993;8:389–92.
26. LeGeros RZ. Biodegradation and bioresorption of calcium phosphate ceramics. Clin Mater. 1993;14:65–88.
27. Hong Z, et al. Crystalline hydroxyapatite thin films produced at room temperature-An opposing radio frequency magnetron sputtering approach. Thin Solid Films. 2007;515:6773–80.
28. Liu X, Chu PK, Ding C. Surface modification of titanium, titanium alloys, and related materials for biomedical applications. Mater Sci Eng. 2004;R47:49–121.
29. Yamagishi M, Kuriki S, Song PK, Shigesato Y. Thin film TiO_2 photocatalyst deposited by reactive magnetron sputtering. Thin Solid Films. 2003;442:227–31.
30. Lukaszkowicz K, Dobrzański L. A. Structure and mechanical properties of gradient coatings deposited by PVD technology onto the X40CrMoV5–1 steel substrate. Mater Sci. 2008;43: 3400–7.
31. Qinnan Z, Baoshun L, Xiujian Z, et al. Effect of ratio of oxygen to argon and thermal treatment on the structure and hydrophilicity of TiO_2 thin films coated on glass by DC reactive magnetron sputtering. Rare Met Mater Eng. 2003;32:339–43.
32. Liu B, Zhao X, Zhao Q, Li C, He X. The effect of O_2 partial pressure on the structure and photocatalytic property of TiO_2 films prepared by sputtering. Mater Chem Phys. 2005;90:207–12.
33. Miyagi T, Kamei M, Ogawa T, Mitsuhashi T, Yamazaki A, Sato T. Pulse mode effects on crystallization temperature of titanium dioxide films in pulse magnetron sputtering. Thin Solid Films. 2003;442:32–5.
34. Zywitzki O, Modes T, Sahm H, Frach P, Goedicke K, Gloss D. Structure and properties of crystalline titanium oxide layers deposited by reactive pulse magnetron sputtering. Surf Coat Technol. 2004;180:538–43.
35. Zywitzki O, Modes T, Frach P, Gloss D. Effect of structure and morphology on photocatalytic properties of TiO_2 layers. Surf Coat Technol. 2008;202:2488–93.
36. Kasemanankul P, et al. Low-temperature deposition of (1 1 0) and (1 0 1) rutile TiO2 thin films using dual cathode DC unbalanced magnetron sputtering for inducing hydroxyapatite. Mater Chem Phys. 2009;117:288–93.
37. Murray JL, Wriedt HA. The O-Ti (Oxygen-Titanium) system. Bull Alloy Phase Diagrams. 1987;8(2):148–65.
38. Guerin D, Ismat Shah S. Reactive-sputtering of titanium oxide thin films. J Vac Sci Technol. 1997;15A:712–5.
39. Song PK, Irie Y, Shigesato Y. Crystallinity and photocatalytic activity of TiO_2 films deposited by reactive sputtering with radio frequency substrate bias. Thin Solid Films. 2006;496:121–5.
40. Ohring M. Materials science of thin film: depositions and structure. 2nd ed. San Diego: Academic Press; 2002.
41. Lindahl C, Borchardt P, Lausmaa J, Xia W, Engqvist H. Studies of early growth mechanisms of hydroxyapatite on single crystalline rutile: a model system for bioactive surfaces. J Mater Sci Mater Med. 2010;21:2734–49.